Science Bulletin 64 (2019) 1608–1616

Contents lists available at ScienceDirect

Science Bulletin

journal homepage: www.elsevier.com/locate/scib

Science Bulletin
www.scibull.com

Article

Spontaneous low-temperature crystallization of α-$FAPbI_3$ for highly efficient perovskite solar cells

Taiyang Zhang [a,1], Qiaoling Xu [b,1], Feng Xu [a,1], Yuhao Fu [b], Yong Wang [a], Yanfa Yan [c], Lijun Zhang [b,d,*], Yixin Zhao [a,*]

[a] School of Environmental Science and Engineering, Shanghai Jiao Tong University, Shanghai 200240, China
[b] Key Laboratory of Automobile Materials, Ministry of Education, School of Materials Science and Engineering, Jilin University, Changchun 130012, China
[c] Department of Physics and Astronomy, University of Toledo, Toledo, OH 43606, USA
[d] State Key Laboratory of Superhard Materials, Jilin University, Changchun 130012, China

ARTICLE INFO

Article history:
Received 26 June 2019
Received in revised form 24 July 2019
Accepted 16 August 2019
Available online 28 August 2019

Keywords:
Perovskite solar cells
Spontaneous crystallization
$FAPbI_3$
Two-dimensional (2D) perovskites

ABSTRACT

Formamidinium lead triiodide ($HC(NH_2)_2PbI_3$ or $FAPbI_3$) is a promising light absorber for high-efficiency perovskite solar cells because of its superior light absorption range and thermal stability to $CH_3NH_3PbI_3$ ($MAPbI_3$). Unfortunately, it is difficult to fabricate high-quality $FAPbI_3$ thin films to surpass the $MAPbI_3$-based cells due to easily forming unwanted but more stable yellow δ-phase and thus requiring high annealing-temperature for wanted photovoltaic-active black α-phase. Herein, we reported a novel low-temperature fabrication of highly crystallized α-$FAPbI_3$ film exhibiting uniaxial-oriented nature with large grain sizes up to 2 μm. First-principles energetic calculations predicted that this novel deposition should be ascribed to the formation of a high-energy metastable two-dimensional (2D) intermediate of $MAFAPbI_3Cl$ followed by a spontaneous conversion to α-$FAPbI_3$. The ions exchange reaction during this $MAFAPbI_3Cl$-$FAPbI_3$ conversion account for the perovskite film uniaxial-oriented grown along the (1 1 1) direction. This large-grain and uniaxial-oriented grown α-$FAPbI_3$ based solar cells exhibited an efficiency up to 20.4% accompanying with low density-voltage (*J-V*) hysteresis and high stability.

1. Introduction

Organic-inorganic hybrid halide perovskites have rapidly emerged as one of the most promising semiconductor absorbers for solar cells owing to their unique optoelectronic properties, as well as low-cost and facile fabrication procedure [1–4]. Despite of significant advances, the large-scale fabrication of high-efficiency and high-stability perovskite solar cells is still the main challenge for practical application of hybrid halide perovskites [1–5]. Since the most widely studied $CH_3NH_3PbI_3$ ($MAPbI_3$) perovskite is bothered by both inferior thermal stability (caused by intrinsic phase transformation or decomposition channels) and unideal band gap of ~1.58 eV [6–8], alternative hybrid perovskites with different chemical compositions have been explored [9]. Among them, the $HC(NH_2)_2PbI_3$ ($FAPbI_3$) perovskite and FA-involved mixed-cation perovskites with better thermal stability and narrower band gap (~1.48 eV) emerge as more ideal perovskite solar absorbers [6,10–14]. Although high-efficiency solar cells with power conversion efficiency (PCE) over 23% have been fabricated based on FA-involved mixed-cation/anion perovskites [15], the pure $FAPbI_3$ perovskite solar cells have shown much lower efficiencies (<18%, as summarized in the Table S1 online) [10,12,16–28] and are less reported than the pure $MAPbI_3$ based ones (over 21% efficiency) [29]. This is in contrast to the fact that $FAPbI_3$ with the narrower band gap allows the broader absorption of solar spectrum compared with $MAPbI_3$. This situation is predominantly caused by the difficulty in obtaining high-quality and phase-pure $FAPbI_3$ perovskite films. The main challenge for $FAPbI_3$ perovskite fabrication lies in that the yellow δ-phase (in hexagonal structure) is thermodynamically more stable and apt to form at low temperatures, whereas the photovoltaic active black α-phase (in cubic structure) is usually attained at the annealing temperatures higher than 160 °C due to its substantially larger tolerance factor [17,20,30–32]. Currently, there are several solution chemistry methods to fabricate pure α-$FAPbI_3$ perovskites including additives assisted one step method or some modified two-step

* Corresponding authors.
E-mail addresses: lijun_zhang@jlu.edu.cn (L. Zhang), yixin.zhao@sjtu.edu.cn (Y. Zhao).
[1] These authors contributed equally to this work.

https://doi.org/10.1016/j.scib.2019.08.029
2095-9273/

methods [12,16–21,25–28,33]. However, the high temperature (over 160 °C) annealing is generally necessary in these methods. Such high-temperature annealing not only impacts the growth of high-quality α-$FAPbI_3$ films with large grains but also limits the deposition of perovskites on flexible polymer substrates. Moreover, the high-temperature procedure makes it difficult to grow the uniaxial-oriented films containing less grain boundaries and dislocation defects and thus facilitating carriers transport, as readily achieved in $MAPbI_3$ and MA/FA-involved mixed-cation perovskites [34–36]. The resultantlower efficiencies of phase-pure α-$FAPbI_3$ based cells strongly impeded the further development of the higher-efficiency and higher-stability perovskite solar cells.

Here, we reported a simple one-step low-temperature fabrication of phase-pure α-$FAPbI_3$ perovskite film spontaneously converted from a metastable perovskite intermediate of $MAFAPbI_3Cl$ prepared by solvent engineering. In this approach, the $MAFAPbI_3Cl$ perovskite intermediate with high free energy as revealed by theoretical calculations was obtained by using a designed precursor solutions with stoichiometric ratio of MA:FA:Pb:I:Cl = 1:1:1:3:1 using either MAI + PbI_2 + FACl or FAI + PbI_2 + MACl precursors. We surprisingly find that crystallization of α-$FAPbI_3$ occurs even under room temperature without annealing following the forced formation of metastable $MAFAPbI_3Cl$ perovskite intermediate by anti-solvent extraction. Such one-step spontaneous crystallization leads to formation of the phase-pure α-$FAPbI_3$ films with grain sizes as large as 1–2 μm. Further annealing at the lower temperatures of 120–140 °C to remove by-product MACl significantly enhances the degree of crystallization and film quality. More interestingly, the freshly obtained and the annealed α-$FAPbI_3$ films all exhibit the uniform uniaxial-oriented growth along the (1 1 1) direction. First-principles energetic calculations reveal that the low-temperature crystallization of α-$FAPbI_3$ originates from the spontaneous conversion from the high-energy metastable $MAFAPbI_3Cl$ perovskite intermediate with a two-dimensional (2D) perovskite structure, and the MA/FA cations and Cl/I anions exchange during this process is responsible for the uniaxial-oriented growth. Based on the as-grown highly crystallized uniaxial-oriented α-$FAPbI_3$ perovskite films, we successfully fabricated phase-pure planar $FAPbI_3$ solar cells with 20.39% efficiency and low density-voltage (*J-V*) hysteresis.

2. Materials and methods

2.1. Materials

Formamidinium chloride (FACl), formamidinium iodide (FAI) and methylammonium iodide (MAI) were purchased from Shanghai MaterWin New Materials Co. PbI_2 (99.9985%) and SnO_2 (15% in H_2O colloidal dispersion) were purchased from Alfa Aesar. All the other materials were purchased from Sigma-Aldrich and used as received without any purification.

2.2. Characterization

The crystal structures of the formed perovskite films were characterized on X-ray diffraction (XRD, Shimadzu XRD-6100 diffractometer with Cu Kα radiation). The absorption spectra of the films were measured on a Cary-60 UV–Vis spectrophotometer. The morphologies of the prepared films were characterized by a JSM-7800F Prime scanning electron microscope (SEM) integrated with the NORANTM System 7 Energy-dispersive X-ray spectroscopy (EDS). The photocurrent density-voltage (*J-V*) curves of perovskite solar cells was measured by a Keithley 2401 source meter under simulated AM 1.5G illumination with a scan rate of 0.05 V/s (100 mW/cm^2; Enlitech SS-F5-3A Class AAA Solar Simulator, the light intensity was calibrated by a stand Si cell before test) using a non-reflective metal mask with an aperture area of 0.12 cm^2, the external quantum efficiency (EQE) was measured on a QE-3011 system from Enlitech. All the *J-V* and EQE tests are processed in atmosphere with relative humidity (R.H.) 30%–45%.

2.3. First-principles calculations

All the calculations were carried out using plane-wave pseudopotential methods within density functional theory as implemented in the Vienna *Ab initio* Simulation Package [37,38]. We described the electron-ion interactions using the projected augmented wave pseudopotentials [39] with $2s^22p^2$ for C, $2s^22p^3$ for N, 1s for H, $6s^26p^2$ for Pb, $5s^25p^5$ for I and $3s^23p^5$ for Cl as valence electrons. The generalized gradient approximation formulated by Perdew et al. [40] was used as the exchange correlation functional. We used a kinetic energy cutoff of 520 eV for wave function expansion and *k*-point meshes with spacing of $2\pi \times 0.02$ $Å^{-1}$ or less for electronic Brillouin zone integration. We optimized the equilibrium structural parameters (by fixing lattice shape but relaxing lattice volume and internal ions) of the involved materials through total energy minimization with the residual forces on the atoms converged to below 0.01 eV/Å. To properly take into account the long-range van der Waal interactions that play a nonignorable role in the hybrid perovskites involving organic molecules, the vdW-optB86b functional [41] was adopted.

2.4. Device fabrication

Clean patterned fluorine-doped tin oxide (FTO, TCE 7) glasses were firstly deposited a 20 nm thick compact TiO_2 layer by spray pyrolysis of 0.2 mol/L Ti (IV) bis(ethyl acetoacetate)-diisopropoxide in 1-butanol solution at 450 followed by 1 h annealing at the same temperature. Subsequently, SnO_2 layer was spin coated using 0.75% SnO_2 solution at 4000 r/s for 30 s and then annealed at 150 °C in open air, the substrates were then treated with UV-O_3 for 20 min. For the perovskite precursor solution preparation: 190.8 mg MAI (1.2 mmol), 553 mg PbI_2 (1.2 mmol) and 96.7 mg dimethyl sulfoxide (DMSO) (1.2 mmol) were dissolved in 1 mL dimethylformamide (DMF) to form a 1.2 mol/L solution. The precursor solution was then aged in the N_2-filled glovebox for 0.5 h and then 96 mg FACl (1.2 mmol) powder was added to the aged solution. Perovskite films were deposited by spin coating the precursor solution at 4000 r/s for 20 and 10 s before the ending, 200 μL CB was dropped on the substrate. The films were then taken out from the dry box and annealed at 140 °C for 5 min in atmosphere with ~30% R.H. Then the annealed films were spin coated with a layer of hole transport material (HTM) of 0.1 mol/L spiro-MeOTAD, 0.035 mol/L bis(trifluoromethane) sulfonimide lithium salt (Li-TFSi), and 0.12 mol/L 4-*tert*-butylpyridine (TBP) in chlorobenzene (CB)/acetonitrile (10:1, v:v) solution at 4000 r/min for 20 s. The ~100 nm thick Ag contacts were deposited by thermal evaporation. All the process was operated in a dry box with less than 20% humidity.

3. Results and discussion

Solvent engineering or anti-solvent process has been one of the most widely used method to prepare solar hybrid halide perovskites including FA-based ones [42,43]. The mechanism of such kinetic growth route is to forcedly crystalize or nucleate solute components via a fast solvent extraction. When we attempted to adopt this typical approach to deposit pure $FAPbI_3$ film with PbI_2 + FAI precursor, a greenish $FAPbI_3$ precursor film was firstly obtained and a 170 °C, 10 min annealing procedure is required to convert the

precursor film into a dark red perovskite film. Unfortunately, even after such high-temperature procedure, the purity of obtained $FAPbI_3$ films was poor. As shown in Figs. S1 and S2 (online), although the UV–Vis spectrum and XRD patterns of the synthesized samples show characteristic absorption onset and satellite XRD peak at 13.8° of α-$FAPbI_3$, their intensities are rather weak, and the XRD patterns are accompanied by a characteristic δ-phase peak locating at ~11.8°. Therefore the high-quality, phase-pure α-$FAPbI_3$ films are challenging to be obtained using typical PbI_2 + FAI precursor, consistent with the previous reports [13,17]. To overcome this issue, we successfully designed a novel perovskite recipe precursor of $MAFAPbI_3Cl$ with a stoichiometric ratio of MA:FA:Pb:I:Cl = 1:1:1:3:1 using FACl, MAI, PbI_2 as reaction precursors through solvent engineering. Here we should state that there is no significantly difference between the two precursors of FACl + MAI + PbI_2 or MACl + FAI + PbI_2. In our experiments, the FAI + PbI_2 or MAI + PbI_2 precursors were first dissolved and aged for 0.5 h followed by adding FACl or MACl. The PbI_2 and MAI or FAI would dissolve as colloidal soft framework with $[PbI_3]^-$ pattern surface terminated by solvent molecules and MA^+ or FA^+ cations in solution. As shown in Fig. S3 (online), the UV–Vis spectra of the MAI + PbI_2 and FAI + PbI_2 are almost identical to each other. With the addition of MACl or FACl, these Cl^- anions would coordinate with colloidal frameworks of $[PbI_3]^-$ and split them into colloidal $[PbI_3Cl]^{2-}$ nanosheets. The MAI + PbI_2 + FACl and FAI + PbI_2 + MACl precursors are also identical to each other but show the same blue shift compare to MAI + PbI_2 and FAI + PbI_2 because of the intercalation of Cl. From this viewpoint, there is therefore no difference between the recipes of FACl + PbI_2 + MAI and MACl + PbI_2 + FAI. The schematic illustration for the formation of colloidal $[PbI_3Cl]^{2-}$ nanosheets is listed in Fig. 1a. Surprisingly, the phase-pure α-$FAPbI_3$ perovskite films can be immediately obtained at room temperature without any annealing process. With the CB anti-solvent dropped to extract the precursor, a greenish film was at first forcedly formed. This greenish $MAFAPbI_3Cl$ precursor film then exhibits a dramatic color change from green to red on the time scale of second during spin coating process as shown in Fig. 1b. In contrast, no color change was observed after the anti-solvent dropping into the regular PbI_2 + FAI precursor in our experiments. After the finish of spin coating, a red and uniform film was obtained (insert of Fig. 1c). The UV–Vis spectrum and XRD patterns of the freshly spin-coated films without annealing are listed in Fig. 1c, d. The absorption spectrum onset of the dark red film arises at around 840 nm, consistent with the band gap of α-$FAPbI_3$ (1.48 eV). The film shows two strong characteristic XRD peaks at around 13.8° and ~28°, which could be indexed to the (1 1 1) and (2 2 2) peaks of α-$FAPbI_3$ (in trigonal *P3m1* structure) [44]. Other than the characteristic absorption and XRD features of α-$FAPbI_3$, there appear some unknown peaks in both UV–Vis spectrum and XRD patterns, which could be related to PbI_2-solvent complex similar to previous reports on solvent engineering prepared $FAPbI_3$ or $MAPbI_3$ precursor films [13,42]. These results clearly indicate that the forcedly formed $MAFAPbI_3Cl$ precursor film is at least partially converted into α-$FAPbI_3$ without appearance of any δ-$FAPbI_3$ under room temperature even without thermal annealing. The more interesting finding is that our designed $MAFAPbI_3Cl$ recipe precursor prepared $FAPbI_3$ film shows the even higher characteristic α-phase peak intensity than the 170 °C annealed sample synthesized using the regular PbI_2 + FAI precursor (Fig. S4 online).

Although the freshly spin-coated films exhibit strong characteristics of phase-pure α-$FAPbI_3$, we found that a thermal annealing post-processing further crystalize α-$FAPbI_3$ and remarkably enhance film quality through expelling out solvent and the by-product of MACl from the $MAFAPbI_3Cl$-to-$FAPbI_3$ conversion. To optimize the thermal annealing condition, a thermal gravity analysis (TGA) performed on the evaporated $MAFAPbI_3Cl$ precursor solution. The results (Fig. S5 online) indicate that the weight loss related to MACl by-product becomes fast when annealing temperature is higher than 100 °C. The temperature of 120–140 °C are suitable for the annealing treatment, but the annealing at 140 °C can remove the residual MACl more quickly. We then chose 140 °C as the annealing temperature, accompanying with optimal annealing duration of 5 min (see the optimization process in Fig. S6 online), to fabricate high-quality α-$FAPbI_3$ film. Both UV–Vis spectrum and XRD patterns (Fig. 2a, b) of these annealed films exhibit characteristic features of phase-pure α-$FAPbI_3$ without any traceable δ-phase. Although the absorbance onset is almost the same after annealing, the annealed film clearly exhibits much faster-rising absorption edge and generally enhanced absorbance. More importantly, the annealed films demonstrate high-crystallinity peaks of pure α-$FAPbI_3$, with around 100 times stronger peak intensity than the sample without annealing and the regular PbI_2 + FAI precursor prepared $FAPbI_3$ with 170 °C annealing (Figs. 2b and S4 (online)). By further examining the morphology evolution of the film before and after annealing (with SEM in Fig. 2c), we found that after annealing, the top surface becomes smoother. The compact and the grain boundaries are more distinguished, consistent with its enhanced crystallinity. In order to exclude the impact of possible vacuum induced crystal growth on SEM measurements, we also characterize as deposited $FAPbI_3$ without annealing using atomic force microscopy (Fig. S7 online), which shows the similar grain size as the SEM measurement. It should be pointed out that the grain sizes before and after annealing are almost the same, which indicates the immediate formation of large-grain α-$FAPbI_3$ through the room-temperature crystallization process rather than the annealing induced crystal regrowth. Besides the achieved phase purity and high crystallinity, all the annealed samples show very strong XRD peaks at ~13.8° and ~28.0° corresponding to (1 1 1) and (2 2 2) planes of α-$FAPbI_3$ (in accompany with the visible ~42.6° and ~58.0° peaks corresponding to (3 3 3) and (4 4 4) planes). This indicates the uniform uniaxial-oriented growth along the (1 1 1) direction of the α-$FAPbI_3$ films. Such highly oriented growth of hybrid halide perovskite films has been reported in $MAPbI_3$ [34,35] and mixed cations/anions perovskites [36], but is achieved for the first time here in $FAPbI_3$. Note that even the freshly spin-coated films formed at room temperature display the similar crystallographic properties, especially the (1 1 1) oriented growth as shown in Fig. 1d, though with the lower XRD peaks intensity.

The higher-resolution SEM image in Fig. 2d shows that our annealed α-$FAPbI_3$ films present the large perovskite crystal grain up to 2 μm. Moreover, these large-grain α-$FAPbI_3$ crystals exhibit homogeneous quasi-single-crystal facets and very smooth surface. They are uniformly oriented along the same (1 1 1) direction, in accord with the XRD pattern results (Fig. 2b). Such large-grain and uniaxial-oriented grown α-$FAPbI_3$ films are expected to be greatly beneficial for carriers transport and exaction. In contrast, the grain size of those $FAPbI_3$ films grown from the regular PbI_2 + FAI precursor is only within several hundred nm and the crystals exhibit diverse crystal facets as in typical polycrystalline films (Fig. S8 online). To confirm the films we deposited are pure α-$FAPbI_3$ rather than FA/MA mixed perovskite, we further compared the UV–Vis spectra of our films with that of standard $FAPbI_3$ film prepared by the classical HI assisted method [16] (Fig. S9 online). We found both of two samples show the same absorption onset, evidencing the phase-pure nature of our $FAPbI_3$ films. We note that there is negligible amount of Cl found in the annealed perovskite films as measured by X-ray photoelectron spectroscopy (XPS) analysis (Fig. S10 online), which is similar to previous reported case using some Cl additive [27,45,46].

All the above results demonstrate that the $MAFAPbI_3Cl$ precursor can be exploited to fabricate phase-pure large-grain α-$FAPbI_3$

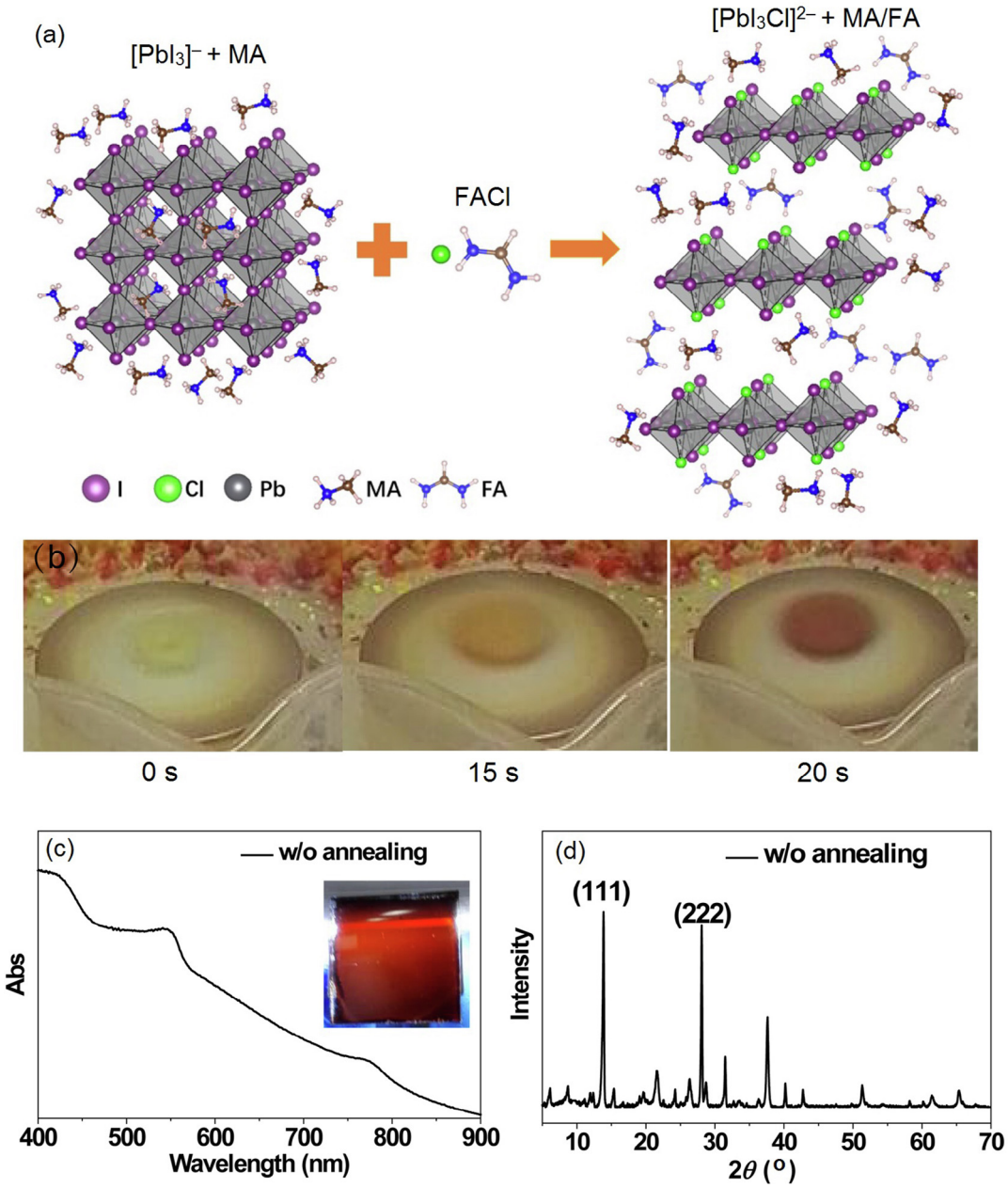

Fig. 1. (Color online) Growth and characterization of the low temperature crystalized $FAPbI_3$ films. (a) Schematic illustration for the formation of colloidal $[PbI_3Cl]^{2-}$ nanosheets. (b) Photos of color changing on the scale of second after anti-solvent dropping during spin coating. UV–Vis spectrum (c) and XRD patterns (d) of freshly spin-coated film without thermal annealing (a red and uniform film as in the inset image of (c)).

perovskite films with desired uniaxial-growth nature at low temperatures. First-principles calculations were performed to unravel the underlying mechanism. We started from the energetic calculations of the normal synthetic routes for $MAPbI_3$ and $FAPbI_3$, i.e., using PbI_2 + MAI and PbI_2 + FAI as precursors, respectively. As shown in Fig. 3a, the obtained energies of $MAPbI_3$ and PbI_2 + MAI are rather close, with a small energy difference of ~22 meV per Pb [47]. The nearly degenerate energies of reaction precursors and final products generally mean that the reaction is prone to occur (though the products could not be thermodynamically stable). This is consistent with the fact that $MAPbI_3$ is found to be easy-to-make from the PbI_2 + MAI precursor and even simple mechanic mixing of PbI_2 and MAI powders can form a fraction of $MAPbI_3$ crystals at room temperature. Turning to the $FAPbI_3$ case (Fig. 3b), while α-$FAPbI_3$ shows a quite large energy difference of ~105 meV from PbI_2 + FAI, δ-$FAPbI_3$ has a slightly lower energy (−6 meV) than PbI_2 + FAI. This accords with the known experimental finding that the formation of α-$FAPbI_3$ needs high-temperature annealing to overcome the larger reaction barrier, whereas δ-$FAPbI_3$ can be easily formed at low temperatures. These results indicate that our first principle calculations are reliably capable to depict the energetics of synthetic routes for $MAPbI_3$ and $FAPbI_3$ perovskites.

As we mentioned, our FACl + PbI_2 + MAI precursor solution is consisted of colloidal $[PbI_3Cl]^{2-}$ nanosheet with FA^+ and MA^+ cations. For our designed growth, we propose that these $[PbI_3Cl]^{2-}$ nanosheets and FA^+/MA^+ cations in precursor solution would be forcedly extracted so fast once the anti-solvent is dropped that they would completely react and form an intermediate of $MAFAPbI_3Cl$, which exhibits a structure of 2D perovskite [48].

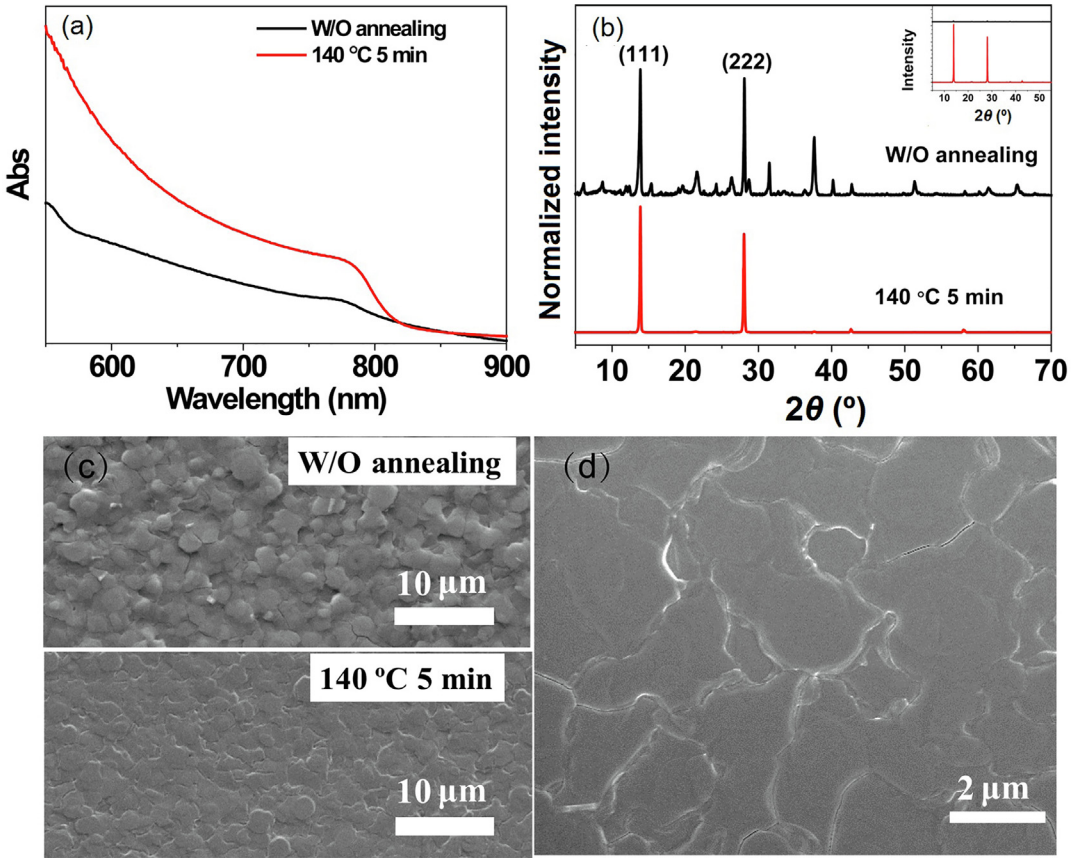

Fig. 2. (Color online) Characterization of the fabricated $FAPbI_3$ perovskite films before and after annealing. (a) UV–Vis spectrum, (b) normalized XRD patterns (inset is the raw XRD patterns), (c) SEM images of the $FAPbI_3$ films before and after annealing at 140 °C for 5 min. (d) SEM image of the film annealed at 140 °C for 5 min with higher resolution.

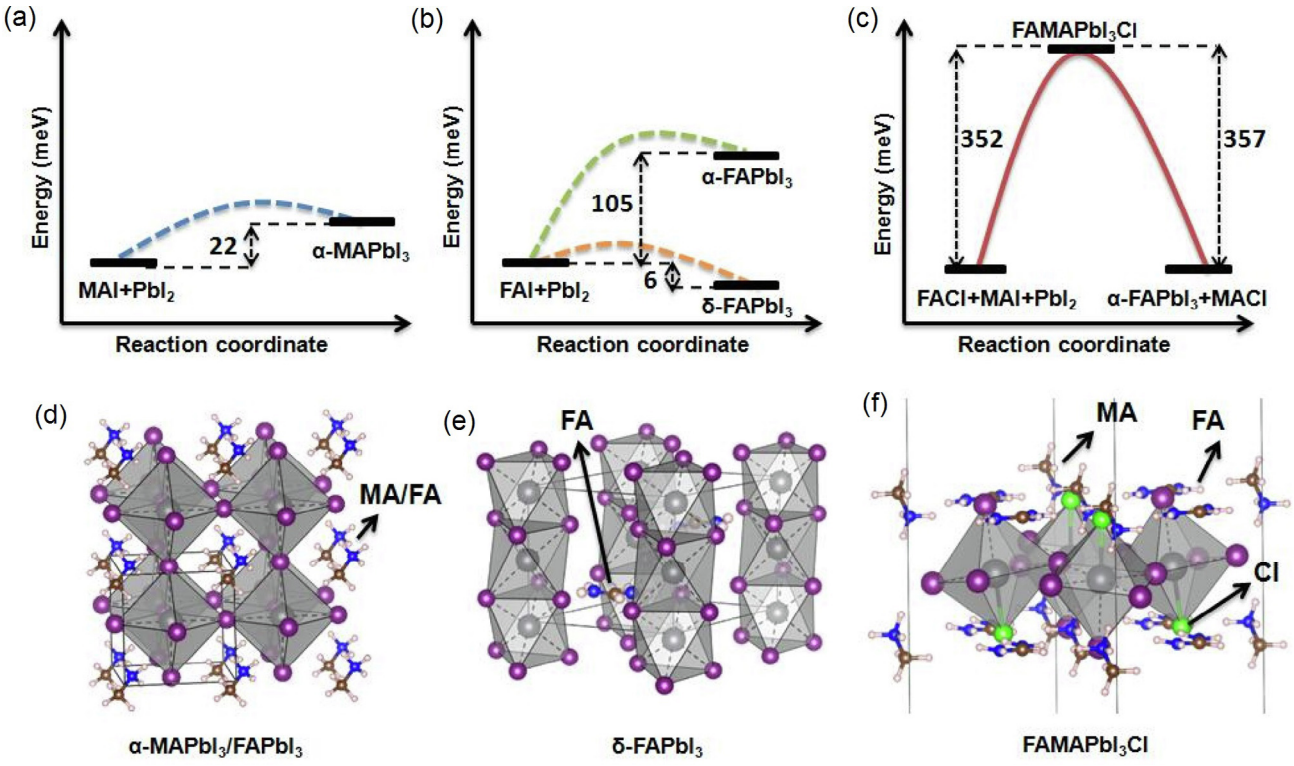

Fig. 3. (Color online) First-principles energetic calculations for $MAPbI_3$ and $FAPbI_3$. Calculated free energies for various reaction precursors and formed products. (a) MAI + PbI_2 and α-$MAPbI_3$, (b) PbI_2 + FAI and α-$FAPbI_3$, δ-$FAPbI_3$, (c) FACl + MAI + PbI_2 and α-$FAPbI_3$. The energy is in meV/Pb. (d)–(f) Crystal structures of α-$MAPbI_3$/α-$FAPbI_3$, δ-$FAPbI_3$ and 2D $MAFAPbI_3Cl$ perovskites.

The immediate formation of 2D $MAFAPbI_3Cl$ perovskite is reasonable by considering that the 2D perovskiter frame like colloidal $[PbI_3Cl]^{2-}$ nanosheet with $Pb(I_4Cl_2)$ octahedra unit is coordinated with FA^+ and MA^+ cations and solvent molecules in solution and the anti-solvent process will extract most solvent molecules. The theoretical calculation has suggested the 2D $MAFAPbI_3Cl$ perovskite exhibit > 2.4 eV band gap in Fig. S11 (online). Therefore, the observed fact that an instantaneous greenish film was firstly observed just after the anti-solvent dropped in, and has been highly related to the formed metastable 2D $MAFAPbI_3Cl$ perovskite. Calculations in Fig. 3c indicate that the energy of intermediate product of 2D $MAFAPbI_3Cl$ is more than 350 meV per Pb and higher than both raw materials $FACl + PbI_2 + MAI$ and the final products α-$FAPbI_3 + MACl$. That is to say, the intermediate 2D $MAFAPbI_3Cl$ is highly energetically unstable. Following its forced formation assisted by the anti-solvent dropping during spin coating, it would transform dramatically to the final $FAPbI_3 + MACl$ products. This explains the second scale of color change from green to red as observed in Fig. 1a. Moreover, such synthetic route through the intermediate 2D $MAFAPbI_3Cl$ perovskite would inhibit formation of δ-$FAPbI_3$, but prefer to α-$FAPbI_3$ due to the steric effect as demonstrated in Fig. 3d–f. The phase change from 2D $MAFAPbI_3Cl$ to α-$FAPbI_3$ may not be governed by the energetics, but the kinetics since forming the δ-$FAPbI_3$ requires additional rearrangement of the PbI_6 octahedra. Therefore, the fast formation of phase-pure α-$FAPbI_3$ at room temperature is originated from the spontaneous conversion from the high-energy metastable 2D $MAFAPbI_3Cl$ perovskite intermediate forcedly formed by solvent engineering.

Further calculations of intermediate 2D $MAFAPbI_3Cl$ by considering different arrangements of I/Cl ions indicate that the structure with cross-distribution of Cl at the bilateral anion sites (Fig. 3f) are energetically favored (Fig. S12 online). The diffusion energy I/Cl anions exchange is lower than the I/I anion exchange as shown in Fig. S13 (online). The MACl is also more volatile than the FACl, MAI or FAI. Therefore, we can explain the uniform uniaxial-oriented growth along the (1 1 1) direction during the 2D $MAFAPbI_3Cl$ to α-$FAPbI_3$ conversion as demonstrated in Fig. 4. When 2D $MAFAPbI_3Cl$ interlayers react, both the I/Cl anions and MA/FA cations exchange leads to the 45° tilt of lattice. During this process, the MACl by-products are expelled out. Consequently, a high-quality (1 1 1) oriented α-$FAPbI_3$ film is formed after annealing treatment to remove all MACl. All these theoretical results reveal the key role of emergence of the high-energy metastable 2D $MAFAPbI_3Cl$ perovskite intermediate in fabricating phase-pure uniaxial-oriented α-$FAPbI_3$ films. The driving force for forming the metastable 2D $MAFAPbI_3Cl$ intermediate is solvent engineering, i.e., anti-solvent extraction. This is further supported by our experimental finding that the same 2D perovskite recipe precursor of $MAFAPbI_3Cl$ without anti-solvent extraction can never form phase-pure α-$FAPbI_3$ at room temperature (Fig. S14 online). This is understandable since without formation of the metastable 2D $MAFAPbI_3Cl$ intermediate, the synthesis procedure is then similar to the previously reported additive (MACl) assisting one-step method [19,49,50], in which the unwanted δ-$FAPbI_3$ cannot be avoided and has to slowly convert into α-$FAPbI_3$ through phase transformation driven by the thermal annealing induced anions and cations exchange reaction [19,49,50]. Based on such the above theoretical calculation, we also theoretically and experimentally investigate another two precursors of $MACl + MAI + PbI_2$ and $FACl + FAI + PbI_2$ to support our proposed hypothesis. The theoretical calculation suggested that the 2D MA_2PbI_3Cl perovskite intermediate of $MACl + MAI + PbI_2$ even show a little higher energy than the final product of $MAPbI_3$ and MACl (Fig. S15 online). Experimentally, we also observed the $MACl + MAI + PbI_2$ precursor would turn into large grain size and orient the grown $MAPbI_3$ perovskite films with efficiency > 18% as shown in Figs. S16 and S17 (online). In contrast, we found that it is impossible to form a 2D FA_2PbI_3Cl perovskite because its energy is really too high compared to that of $FAPbI_3 + FACl$ (Fig. S15 online). Experimentally, we have observed the formation of phase pure black $FAPbI_3$ films and the corresponding device exhibits low efficiency (Figs. S16 and S17 online).

Using the abovementioned high quality uniaxial-oriented α-$FAPbI_3$ perovskite films, we then fabricated a modified planar configuration perovskite solar cell devices. In this modified planar configuration, the regular compact TiO_2 layer was replaced by a combination of SnO_2 nanoparticles film and compact TiO_2 because this combined electron transfer layer has better electron extraction and transfer properties with enhanced reproducibility to avoid short circuit [51]. The α-$FAPbI_3$ perovskite solar cell devices exhibited a highly competitive PCE and a small *J-V* hysteresis. The champion device exhibits PCE up to 20.39% under reverse scan and 19.56% under forward scan. Fig. 5a shows the *J-V* of the champion α-$FAPbI_3$ perovskite solar cell device, which shows a V_{oc} of 1.06 V, a J_{sc} of 23.95 mA/cm^2 and a FF of 0.81 under reverse scan measurement. In contrast, the champion device based on the $FAPbI_3$ film

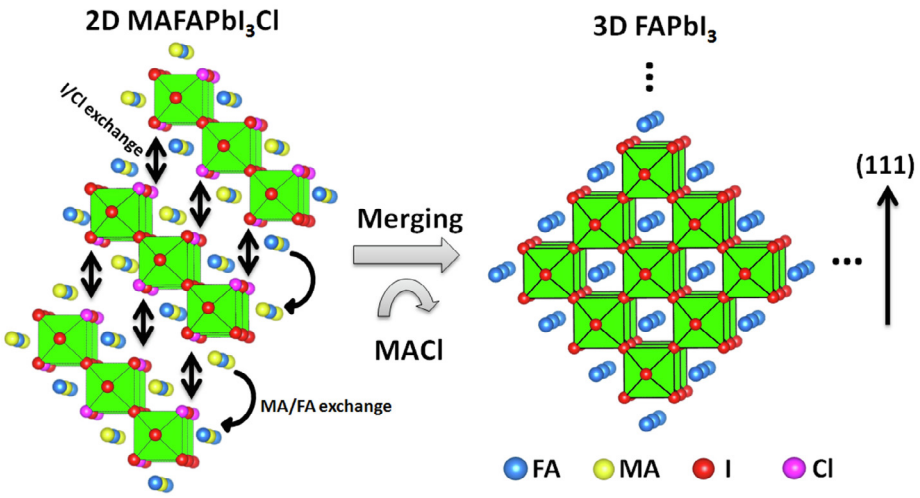

Fig. 4. (Color online) Schematic of spontaneous structural conversion from the 2D $MAFAPbI_3Cl$ perovskite intermediate to the (1 1 1) uniaxial oriented 3D α-$FAPbI_3$ perovskite. As demonstrated the I/Cl anions and MA/FA cations exchange plays important role in the uniaxial-oriented growth.

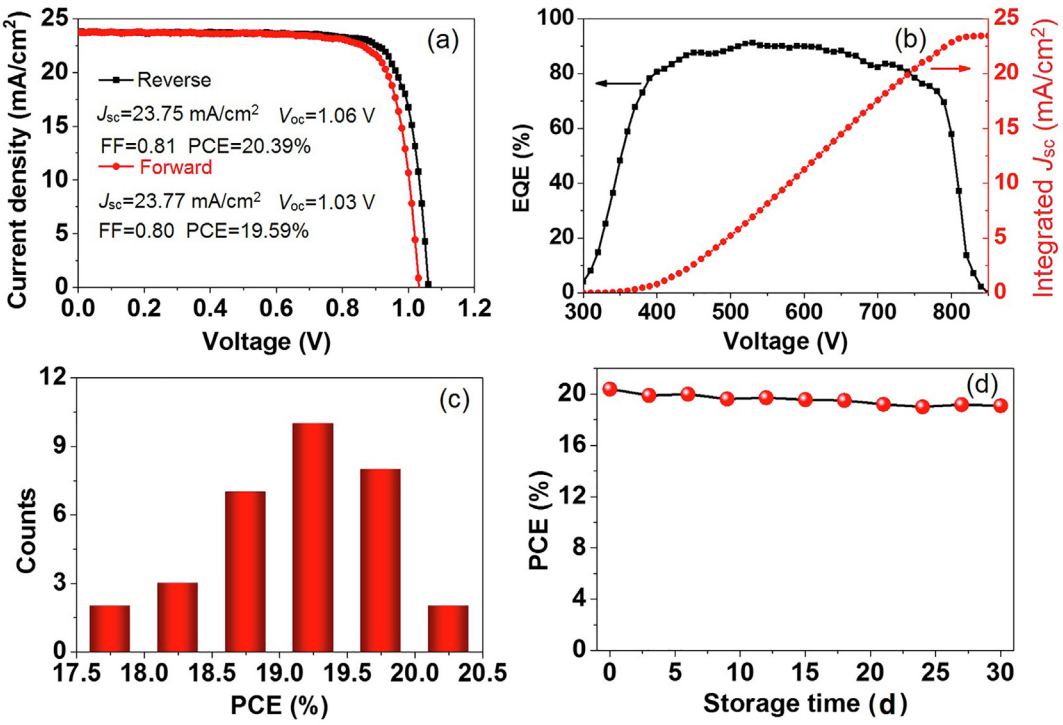

Fig. 5. (Color online) Performance of the fabricated $FAPbI_3$ based solar cell devices. (a) The *J-V* curves. (b) The EQE of the champion solar cell. (c) Statistics of PCEs from 32 cells based our recipe. (d) The PCE of the champion device as a function of storage time (in dark desiccator).

fabricated by typical PbI_2 + FAI precursor is only around ~15% (Fig. S18 online). The EQE curve of the champion device in Fig. 5b exhibited a high EQE value and agrees well with UV–Vis spectra, and the integrated J_{sc} by EQE measurement matched with the J_{sc} obtained from *J-V* measurement. The champion devices show a high stable output at maximum point (19.8%) (Fig. S19 online). Other than the high efficiency for champion device, our α-$FAPbI_3$ perovskite solar cells also exhibited high reproducibility as shown in Fig. 5c. Furthermore, our α-$FAPbI_3$ based device exhibited good stability, and the champion device could maintain the ~19% PCE after storage in a desiccator for 30 d as shown in Fig. 5d. We also tested the photo-stability of our device and the un-encapsulated device could retain over 95% of its initial PCE even after 700 h illumination (Fig. S20 online).

4. Conclusions

In summary, we developed a one-step low-temperature fabrication method to grow highly crystallized phase-pure α-$FAPbI_3$ perovskites with micron-size large gain. The key procedure is to exploit the solvent engineering strategy through a designed recipe precursor with stoichiometric ratio of MA:FA:Pb:I:Cl = 1:1:1:3:1 using MAI + PbI_2 + FACl precursors. This leads to the formation of a metastable 2D $MAFAPbI_3Cl$ perovskite intermediate with high free energy as revealed by first-principles calculations that spontaneously transforms to α-$FAPbI_3$ on the second time scale. The fast formation of δ-phase free $FAPbI_3$ perovskite even occured under room temperature. Further annealing at the lower temperatures of 120–140 °C significantly enhances film quality by eliminating MACl by-product. Equally importantly, the fabricated α-$FAPbI_3$ film exhibits highly uniaxial (1 1 1) oriented nature favorable for carriers transport. Theoretical calculations suggest the ions exchange process during the conversion from metastable 2D $MAFAPbI_3Cl$ to α-$FAPbI_3$ is responsible for the (1 1 1) oriented growth. Finally, the high-quality phase-pure α-$FAPbI_3$ perovskite based solar cells exhibit high reproducibility and high performance, and the champion device has an efficiency > 20% in company with a small *J-V* hysteresis. The proposed approach to achieve the highly uniaxial oriented growth and low-temperature formation of crystallized phase-pure α-$FAPbI_3$ would be a promising strategy for synthesize $FAPbI_3$-based mixed halides and other hybrid halide perovskites for high-performance solar cell fabrication.

Conflict of interest

The authors declare that they have no conflict of interest.

Acknowledgments

Yixin Zhao acknowledges the support of the National Natural Science Foundation of China (21777096, 51861145101) and Huoyingdong Grant (151046). Lijun Zhang acknowledges the support of the National Natural Science Foundation of China (61722403, 11674121), and the National Key Research and Development Program of China (2016YFB0201204). Taiyang Zhang acknowledges the support of The Initiative Postdocs Supporting Program (BX20180185) and China Postdoctoral Science Foundation (2018M640387).

Author contributions

Yixin Zhao and Lijun Zhang designed and directed the research. Taiyang Zhang, Feng Xu, and Yong Wang fabricated and characterized the perovskite thin films and devices. Qiaoling Xu and Yuhao Fu performed the theoretical calculations. Yixin Zhao, Taiyang Zhang, Feng Xu, Lijun Zhang, and Yanfa Yan analyzed the results and wrote the manuscript with inputs from all authors.

Appendix A. Supplementary data

Supplementary data to this article can be found online at https://doi.org/10.1016/j.scib.2019.08.029.

References

[1] Park N-G, Grätzel M, Miyasaka T, et al. Towards stable and commercially available perovskite solar cells. Nat Energy 2016;1:16152.
[2] Zhang W, Eperon GE, Snaith HJ. Metal halide perovskites for energy applications. Nat Energy 2016;1:16048.
[3] Green MA, Ho-Baillie A, Snaith HJ. The emergence of perovskite solar cells. Nat Photon 2014;8:506–14.
[4] Correa-Baena J-P, Saliba M, Buonassisi T, et al. Promises and challenges of perovskite solar cells. Science 2017;358:739–44.
[5] Zhao Y, Zhu K. Organic-inorganic hybrid lead halide perovskites for optoelectronic and electronic applications. Chem Soc Rev 2016;45:655–89.
[6] Amat A, Mosconi E, Ronca E, et al. Cation-induced band-gap tuning in organohalide perovskites: interplay of spin-orbit coupling and octahedra tilting. Nano Lett 2014;14:3608–16.
[7] Quarti C, Mosconi E, Ball JM, et al. Structural and optical properties of methylammonium lead iodide across the tetragonal to cubic phase transition: implications for perovskite solar cells. Energy Environ Sci 2016;9:155–63.
[8] Juarez-Perez EJ, Hawash Z, Raga SR, et al. Thermal degradation of $CH_3NH_3PbI_3$ perovskite into NH_3 and CH_3I gases observed by coupled thermogravimetry-mass spectrometry analysis. Energy Environ Sci 2016;9:3406–10.
[9] Li W, Wang Z, Deschler F, et al. Chemically diverse and multifunctional hybrid organic-inorganic perovskites. Nat Rev Mater 2017:16099.
[10] Pang S, Hu H, Zhang J, et al. $NH_2CH{=}NH_2PbI_3$: an alternative organolead iodide perovskite sensitizer for mesoscopic solar cells. Chem Mater 2014;26:1485–91.
[11] Koh TM, Fu K, Fang Y, et al. Formamidinium-containing metal-halide: an alternative material for near-ir absorption perovskite solar cells. J Phys Chem C 2014;118:16458–62.
[12] Lee J-W, Seol D-J, Cho A-N, et al. High-efficiency perovskite solar cells based on the black polymorph of $HC(NH_2)_2PbI_3$. Adv Mater 2014;26:4991–8.
[13] Jeon NJ, Noh JH, Yang WS, et al. Compositional engineering of perovskite materials for high-performance solar cells. Nature 2015;517:476–80.
[14] Haruyama J, Sodeyama K, Han L, et al. First-principles study of ion diffusion in perovskite solar cell sensitizers. J Am Chem Soc 2015;137:10048–51.
[15] Jiang Q, Zhao Y, Zhang X, et al. Surface passivation of perovskite film for efficient solar cells. Nat Photon 2019;13:460–6.
[16] Eperon GE, Stranks SD, Menelaou C, et al. Formamidinium lead trihalide: a broadly tunable perovskite for efficient planar heterojunction solar cells. Energy Environ Sci 2014;7:982–8.
[17] Li Z, Yang M, Park J-S, et al. Stabilizing perovskite structures by tuning tolerance factor: formation of formamidinium and cesium lead iodide solid-state alloys. Chem Mater 2015;28:284–92.
[18] Wang F, Yu H, Xu HH, et al. $HPbI_3$: a new precursor compound for highly efficient solution-processed perovskite solar cells. Adv Funct Mater 2015;25:1120–6.
[19] Wang Z, Zhou Y, Pang S, et al. Additive-modulated evolution of $HC(NH_2)_2PbI_3$ black polymorph for mesoscopic perovskite solar cells. Chem Mater 2015;27:7149–55.
[20] Wozny S, Yang M, Nardes AM, et al. Controlled humidity study on the formation of higher efficiency formamidinium lead triiodide-based solar cells. Chem Mater 2015;27:4814–20.
[21] Aguiar JA, Wozny S, Holesinger TG, et al. *In situ* investigation of the formation and metastability of formamidinium lead tri-iodide perovskite solar cells. Energy Environ Sci 2016;9:2372–82.
[22] Song J, Hu W, Wang X-F, et al. $HC(NH_2)_2PbI_3$ as a thermally stable absorber for efficient ZnO-based perovskite solar cells. J Mater Chem A 2016;4:8435–43.
[23] Wang F, Geng W, Zhou Y, et al. Phenylalkylamine passivation of organolead halide perovskites enabling high-efficiency and air-stable photovoltaic cells. Adv Mater 2016;28:9986–92.
[24] Yang S, Liu W, Zuo L, et al. Thiocyanate assisted performance enhancement of formamidinium based planar perovskite solar cells through a single one-step solution process. J Mater Chem A 2016;4:9430–6.
[25] Zhou Z, Pang S, Ji F, et al. The fabrication of formamidinium lead iodide perovskite thin films via organic cation exchange. Chem Commun 2016;52:3828–31.
[26] Fu Y, Wu T, Wang J, et al. Stabilization of the metastable lead iodide perovskite phase via surface functionalization. Nano Lett 2017;17:4405–14.
[27] Li G, Zhang T, Xu F, et al. A facile deposition of large grain and phase pure α-$FAPbI_3$ for perovskite solar cells via a flash crystallization. Mater Today Energy 2017;5:293–8.
[28] Pool VL, Dou B, Van Campen DG, et al. Thermal engineering of $FAPbI_3$ perovskite material via radiative thermal annealing and *in situ* XRD. Nat Commun 2017;8:14075.
[29] Shin SS, Yeom EJ, Yang WS, et al. Colloidally prepared La-doped $BaSnO_3$ electrodes for efficient, photostable perovskite solar cells. Science 2017;356:167–71.
[30] Stoumpos CC, Malliakas CD, Kanatzidis MG. Semiconducting tin and lead iodide perovskites with organic cations: phase transitions, high mobilities, and near-infrared photoluminescent properties. Inorg Chem 2013;52:9019–38.
[31] Zhou Y, Kwun J, Garces HF, et al. Observation of phase-retention behavior of the $HC(NH_2)_2PbI_3$ black perovskite polymorph upon mesoporous TiO_2 scaffolds. Chem Commun 2016;52:7273–5.
[32] Zhumekenov AA, Saidaminov MI, Haque MA, et al. Formamidinium lead halide perovskite crystals with unprecedented long carrier dynamics and diffusion length. ACS Energy Lett 2016;1:32–7.
[33] Yang WS, Noh JH, Jeon NJ, et al. High-performance photovoltaic perovskite layers fabricated through intramolecular exchange. Science 2015;348:1234–7.
[34] Ji F, Pang S, Zhang L, et al. Simultaneous evolution of uniaxially oriented grains and ultralow-density grain-boundary network in $CH_3NH_3PbI_3$ perovskite thin films mediated by precursor phase metastability. ACS Energy Lett 2017;2:2727–33.
[35] Long M, Zhang T, Zhu H, et al. Textured $CH_3NH_3PbI_3$ thin film with enhanced stability for high performance perovskite solar cells. Nano Energy 2017;33:485–96.
[36] Kim DH, Park J, Li Z, et al. 300% Enhancement of carrier mobility in uniaxial-oriented perovskite films formed by topotactic-oriented attachment. Adv Mater 2017;29:1606831.
[37] Kresse G, Furthmüller J. Efficiency of *ab-initio* total energy calculations for metals and semiconductors using a plane-wave basis set. Comp Mater Sci 1996;6:15–50.
[38] Kresse G, Furthmüller J. Efficient iterative schemes for *ab initio* total-energy calculations using a plane-wave basis set. Phys Rev B 1996;54:11169–86.
[39] Blöchl PE. Projector augmented-wave method. Phys Rev B 1994;50:17953–79.
[40] Perdew JP, Burke K, Ernzerhof M. Generalized gradient approximation made simple. Phys Rev Lett 1996;77:3865–8.
[41] Klimeš J, Bowler DR, Michaelides A. Van der waals density functionals applied to solids. Phys Rev B 2011;83:195131.
[42] Jeon NJ, Noh JH, Kim YC, et al. Solvent engineering for high-performance inorganic-organic hybrid perovskite solar cells. Nat Mater 2014;13:897–903.
[43] Galkowski K, Mitioglu A, Miyata A, et al. Determination of the exciton binding energy and effective masses for methylammonium and formamidinium lead tri-halide perovskite semiconductors. Energy Environ Sci 2016;9:962–70.
[44] Qifeng H, Sang-Hoon B, Pengyu S, et al. Single crystal formamidinium lead iodide ($FAPbI_3$): insight into the structural, optical, and electrical properties. Adv Mater 2016;28:2253–8.
[45] Jiang Q, Zhang L, Wang H, et al. Enhanced electron extraction using SnO_2 for high-efficiency planar-structure $HC(NH_2)_2PbI_3$-based perovskite solar cells. Nat Energy 2016;2:16177.
[46] Zhao Y, Zhu K. CH_3NH_3Cl-assisted one-step solution growth of $CH_3NH_3PbI_3$: structure, charge-carrier dynamics, and photovoltaic properties of perovskite solar cells. J Phys Chem C 2014;118:9412–8.
[47] Yang D, Lv J, Zhao X, et al. Functionality-directed screening of Pb-free hybrid organic-inorganic perovskites with desired intrinsic photovoltaic functionalities. Chem Mater 2017;29:524–38.
[48] Li G, Zhang T, Guo N, et al. Ion-exchange-induced 2D–3D conversion of $HMA_{1-x}FA_xPbI_3Cl$ perovskite into a high-quality $MA_{1-x}Fa_xPbI_3$ perovskite. Angew Chem Int Ed 2016;55:13460–4.
[49] Liu J, Shirai Y, Yang X, et al. High-quality mixed-organic-cation perovskites from a phase-pure non-stoichiometric intermediate FAI_{1-x}-PbI_2 for solar cells. Adv Mater 2015;27:4918–23.
[50] Li C, Zhou Y, Wang L, et al. Methylammonium-mediated evolution of mixed-organic-cation perovskite thin films: a dynamic composition-tuning process. Angew Chem Int Ed 2017;56:7674–8.
[51] Song S, Kang G, Pyeon L, et al. Systematically optimized bilayered electron transport layer for highly efficient planar perovskite solar cells (η = 21.1%). ACS Energy Lett 2017:2667–73.

Taiyang Zhang is a postdoctoral researcher in Shanghai Jiao Tong University. He obtained his Ph.D. degree from Shanghai Jiao Tong University in 2018. His research interests focus on the synthesis of lead halide perovskite photoelectric materials, solar cell fabrications and their physical and chemical nature.

Lijun Zhang obtained his B.S. degree at Northeast Normal University (2003), and completed his Ph.D. degree at Jilin University (2008). As a postdoctoral researcher, he worked at Oak Ridge National Laboratory (2008–2010) and National Renewable Energy Laboratory (2010–2013). He then became a research assistant professor at University of Colorado at Boulder (2013). In 2014, he joined Jilin University as professor. The current interests focus on materials by design and band structures engineering of functional semiconductors for optoelectronic applications.

Yixin Zhao is a professor at Shanghai Jiao Tong University. He obtained his Ph.D. degree from Case Western Reserve University in 2010 followed by working as a postdoctoral fellow at Penn State University and National Renewable Energy Laboratory. His current research interests focus on perovskite solar cells, water splitting cells and functional materials for solar energy conversion and environmental remediation application.